Ente per le Nuove tecnologie,
l'Energia e l'Ambiente

Ministero dello Sviluppo Economico

RICERCA SISTEMA ELETTRICO

Numerical Analysis of Liquid Fuel and Coal Water Slurry Combustion in an Innovative Reactor

A. Di Nardo, G. Calchetti, S. Giammartini, G. Mongibello, C. Mongiello

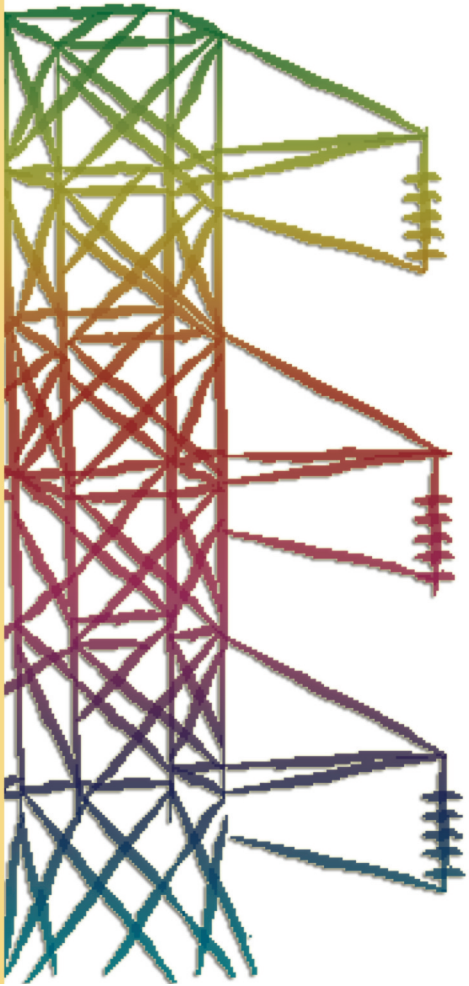

Report RSE/2009/92

Ente per le Nuove tecnologie,
l'Energia e l'Ambiente

Ministero dello Sviluppo Economico

RICERCA SISTEMA ELETTRICO

Numerical Analysis of Liquid Fuel and Coal Water Slurry Combustion in an Innovative Reactor

A. Di Nardo, G. Calchetti, S. Giammartini, G. Mongibello, C. Mongiello

Report RSE/2009/92

NUMERICAL ANALYSIS OF LIQUID FUEL AND COAL WATER SLURRY COMBUSTION IN AN INNOVATIVE REACTOR

A. Di Nardo, G. Calchetti, S. Giammartini, G. Mongibello, C. Mongiello (ENEA)

Aprile 2009

Report Ricerca Sistema Elettrico
Accordo di Programma Ministero dello Sviluppo Economico - ENEA
Area: Produzione e fonti energetiche
Tema: Tecnologie innovative per migliorare i rendimenti di conversione delle centrali a polverino di carbone - Sviluppo di un sistema di combustione di tipo "flameless" per impianti di produzione di elettricità con ridottissimi livelli di emissione di inquinanti e CO_2
Responsabile Tema: Stefano Giammartini, ENEA

NUMERICAL ANALYSIS OF LIQUID FUEL AND COAL WATER SLURRY COMBUSTION IN AN INNOVATIVE REACTOR

A. Di Nardo, G. Calchetti, S. Giammartini, G. Mongibello, C. Mongiello

ENEA - Italian National Agency for new Technologies, Energy and the Environment
Casaccia (Rome) – ITALY

antonio.dinardo@casaccia.enea.it

Abstract
A series of numerical simulations have been done on a special kind of industrial combustor, by mean of commercial CFD software. It is a chemical oxidation reactor for disposal of industrial and hazardous waste. Results are relative to different working condition, in the case of liquid and coal water slurry fuel.

1 INTRODUCTION

The combustion chamber analysed is designed to burn generically waste fuel. It is then necessary guarantee maximum efficiency and ensure complete destruction of all possible pollutants. This is obtained through temperature levels over 2000°C. The particular uniformity of the reaction conditions is strengthened by the recirculation of reaction gasses which, after being cooled, are recycled with oxygen and re-introduced in the reactor. The thermal content of flue gasses is then used for steam production. Since the working condition adopted, a flameless combustion could be present. In flameless oxidation mode, the feeding of oxidising air and fuel gas is performed separately with high injection velocities and this represents an extreme staging of combustion. The high temperature of the recirculated combustion products is used to initiate and maintain this mode of combustion. The flame can then no longer be seen and combustion is, for the most part, distributed throughout the volume of the combustion chamber. The relative homogeneity in temperature and in composition of the combustion chamber is a notable characteristic of the process. As a result of the reduction of temperature peaks in the flame, the mean temperature level of the furnace zone can be increased, reducing NOx, without leading to local overheating in the vicinity of the burners. The heat transfer to the product can thus be considerably increased. In addition, the noise level induced by the combustion is greatly reduced.

2 SIMULATIONS

The reactor has a cylindrical shape (Ø=1 m, L=5.3 m) and recirculated gasses, enriched with oxygen, are introduced through an annular duct provided of swirling blades (fig. 1). At the centre there is the fuel duct, which is transported by water vapour used like propellant. Fuel is injected as particles of large dimensions and at high velocity, in the way to obtain a fine atomisation.

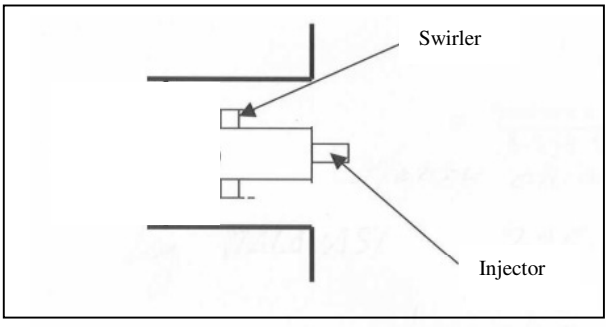

Figure 1. Burner.

Some CFD simulations for different working condition have been executed, using liquid and coal water slurry as fuel, by mean of FLUENT® code (V6.3).
In the first case combustion has been modelled with the eddy dissipation concept model, using a reduced reaction mechanism.
In the second case a three steps reaction scheme has been adopted, with the eddy dissipation model.
The k-ε realizable model has been chosen for turbulence while the Discrete Ordinate model has been adopted for radiative heat transfer.
In the k-ε model [1] two additional equations are solved, one for the turbulence kinetic energy (k) and one for its dissipation rate (ε). The first is an exact equation, while the second one is obtained using physical reasoning. The term "realizable" [2] means that the model satisfies certain mathematical constraints on the normal stresses, consistent with the physics of turbulent flows.
The discrete ordinates (DO) radiation model [3] is applicable for any optical thickness. It transforms the radiative heat transfer equation into a transport equation for radiation intensity in the spatial coordinates (x; y; z), which are solved for a finite number of discrete solid angles, each associated with a vector direction $\boldsymbol{s}$ fixed in the global Cartesian system (x; y; z). At the end there are many transport equations as there are directions $\boldsymbol{s}$. Radiative gas properties are modelled by the weighted-sum-of-grey-gases model (WSGGM) [4 ,5]. Particles radiation interaction has been taken into account.

3 DISCRETE PHASE MODELLING

Liquid fuel droplets and coal water slurry particles are simulated as a second discrete phase, added to the continuous phase. The trajectories, the mass and heat transfer of these discrete phase are solved in a Lagrangian reference frame. So the strong coupling between discrete and continuous phases is taken into account: the physics of particles and gasses impact each other. Continuous phase turbulence determines instantaneous turbulent velocity fluctuations on the particle trajectories. The dispersion of particles due to turbulence in the fluid phase has been predicted using the stochastic tracking model: by computing the trajectory for a sufficient number of representative particles, the random effects of turbulence on the particle dispersion is accounted for.

4 LIQUID FUEL COMBUSTION MODELLING

An accurate determination of the drag coefficient is necessary for a realistic spray modelling. Since the droplet varies its shape during the motion, a method that calculates the droplet drag coefficient dynamically has been used. Having considered droplet collisions, after a collision, shape distortion is resetted. An initial spherical droplet moving through a gas, change its shape especially when the Weber number is large, becoming a flat disk for very large Weber. The dynamic drag model [6, 7] accounts for the effects of droplet distortion, linearly varying the drag between that of a sphere and a value of 1.54 corresponding to a disk.
The droplet temperature is calculated from the balance equation of the sensible heat change in the droplet, the convective and latent heat transfer between the droplet and the continuous phase.
Vaporization starts when the temperature of the droplet reaches the vaporization temperature and continues until the droplet reaches the boiling point or until the droplet's volatile fraction is completely consumed. The rate of vaporization is related to the gradient of the vapour concentration between the droplet surface and the bulk gas [8, 9].
The convective boiling of a discrete phase droplet starts when the temperature of the droplet has reached the boiling temperature and while the mass of the droplet exceeds the non-volatile fraction. When the droplet temperature reaches the boiling point, a boiling rate equation is applied [10]. While the droplet boils, its temperature is assumed constant. The energy needed and the mass evaporated, appear as a negative source in the energy equation and a positive source in the transport equation for the specie considered, respectively.
In the analysis conducted the droplet break-up and collision have been considered. For high-Weber-number (high-speed injections) flows the wave model [11, 12] is the most suitable.

The time of break-up and the droplet size are evaluated from a jet stability analysis, considering the fastest-growing Kelvin-Helmholtz instability, enhanced by external forces. The break-up time is determined by the growth rate of the most unstable wave. The child drop size is determined by the wavelength of the most unstable wave. Regarding to droplet collision, the prohibitive computational cost is reduced using the O'Rourke stochastic algorithm [13].

4.1 Results

In the simulations, recirculated products range from 2800 kg/h to 11200 kg/h (28000-5600-11200), at 800 K. Fuel flow rate is 450 kg/h, while oxygen is fixed at 1620 kg/h (with a 10 % in excess). The reactor has been considered adiabatic (indicated AD in the figures) and non adiabatic (with a wall temperature fixed at 1600 K). Heptane has been used as model fuel. The choice of heptane has been necessary because it is the most similar fuel with respect diesel oil, for which a reduced scheme exists. Combustion phenomena have been modelled by eddy-dissipation concept model, with a reduced mechanism made of 41 reactions and 18 species, as reported in table 1. Other combustion model, like eddy dissipation and laminar flamelets, would have been less suitable to capture non equilibrium phenomena in these cases, where, because of the lower concentration of oxygen with respect ambient air and the mass flow rate of recirculated gasses, chemical kinetic time scales are comparable to mixing time scales.

Simulations effectuated in different conditions have the aim of finding that ones which can guarantee uniform temperature inside the combustion chamber and a complete reaction. As one can see from figures and diagrams, larger recirculated mass flow causes a more uniform temperature distribution, without temperature peaks (fig. 2, 3).

Larger recirculation mass flow determines little difference between adiabatic and non adiabatic cases in terms of temperature distribution (fig. 2). However the adiabatic cases are those with the more uniform distribution: after 1 m from the burner, temperature is perfectly uniform (fig. 2, 3). Maximum temperatures registered are obviously relative to the case of lower recirculation, namely 2800 kg/h, reaching 2600 K, while in the case of larger recirculation, temperature doesn't go over 1600 K.

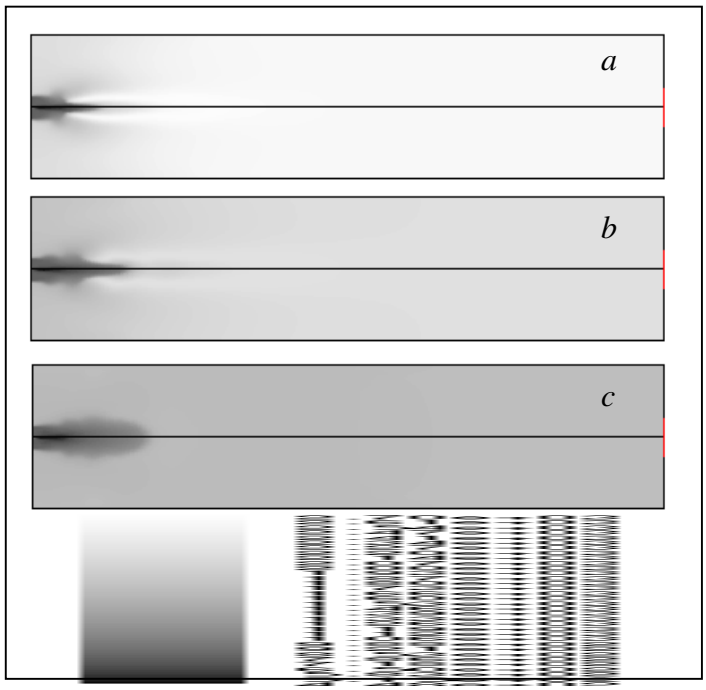

Figure 2. Temperature (K). a)Rec. 2800 kg/h AD. b)Rec. 5600 kg/h AD. c)Rec. 11200 kg/h.

Combustion is ever complete, but in the cases where temperature remains at high values, namely for 2800 and 5600 kg/h in adiabatic conditions, dissociation of CO2 in CO occur (fig. 4). For what concern the flow field, there is an enough internal recirculation inside the reactor just in the first part near the burner, because of the energetic fuel and propellant axial mass flow, introduced at high velocity, which not allow forming large vortices, although the sufficient recirculated flow swirl number.
Despite fuel injection and exhaust high velocity, fine droplets atomisation and exhaust temperature, prevent flame blow out. In fact, even though flame appears long and stretched, reaction front is positioned very close to the burner, extending from 0.3 m to 1.2 m.

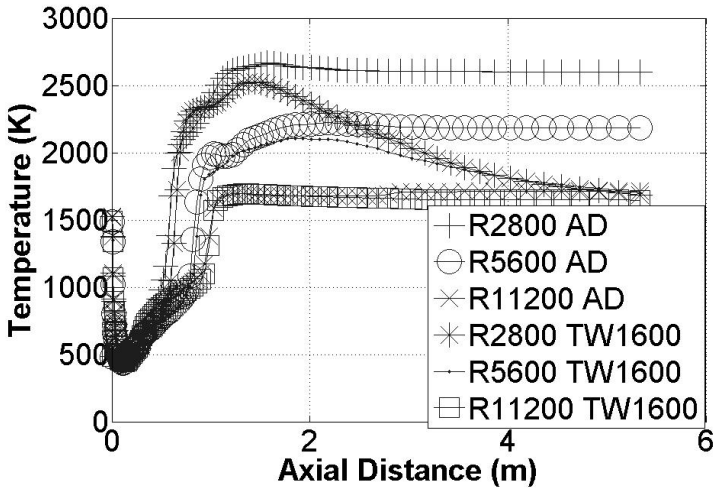

Figure 3. Axial temperature.

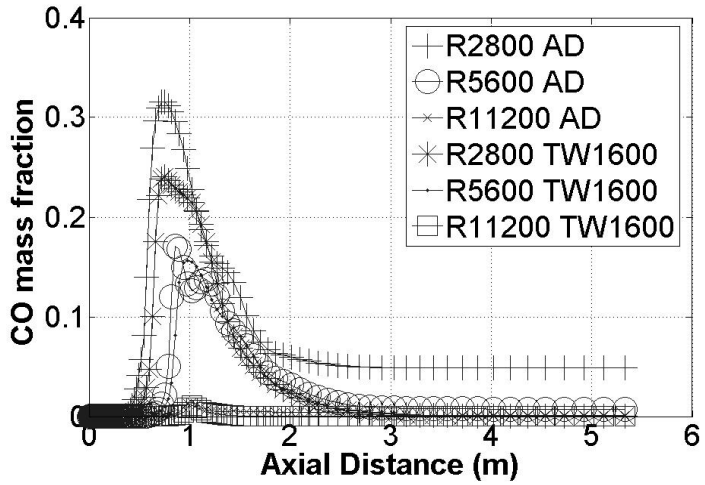

Figure 4. Axial mass fraction of CO.

5 SLURRY PARTICLES PHYSICAL MODELLING

During its motion, slurry particle undergoes several phases: inert heating, water vaporization, coal devolatilization, char combustion. In the model used, devolatilization and surface combustion begin after the water content is completely evaporated.

SPECIES			
H O2 OH O H2 H2O HO2 N2 CO CO2 CH3 CH2O HCO CH3O			
CH3HCO C3H6 C7H16 C7H15			
REACTIONS CAL/MOLE			
!Units are moles, cubic centimeters, seconds, Kelvins, cal/mole.			
H+O2=OH+O	2.2E+14	0.00	16800.
H2+O=OH+H	1.8E+10	1.00	8826.
OH+H2=H2O+H	1.17E+0	1.30	3626.
OH+OH=H2O+O	6.E+08	1.30	0.
H2+M=H+H+M	2.23E+12	0.50	92600.
H+OH+M=H2O+M	7.5E+23	-2.60	0.
H+O2+M=HO2+M	2.1E+18	-1.00	0.
H+O2+N2=HO2+N2	6.7E+19	-1.42	0.
H+HO2=OH+OH	2.5E+14	0.00	1900.
H+HO2=H2+O2	2.5E+13	0.00	700.
O+HO2=OH+O2	4.8E+13	0.00	1000.
OH+HO2=H2O+O2	5.E+13	0.00	1000.
H2+O2=OH+OH	1.7E+13	0.00	47780.
H+O2+O2=HO2+O2	6.7E+19	-1.42	0.
CO+OH=CO2+H	1.51E+07	1.30	-758.
CH3+O=CH2O+H	6.8E+13	0.00	0.
CH2O+H=HCO+H2	3.31E+14	0.00	10500.
CH2O+M=HCO+H+M	3.31E+16	0.00	81000.
CH2O+O=HCO+OH	1.81E+13	0.00	3082.
OH+CH2O=HCO+H2O	7.53E+12	0.00	167.
H+HCO=CO+H2	4.E+13	0.00	0.
HCO+O=CO+OH	1.E+12	0.00	0.
OH+HCO=CO+H2O	5.E+12	0.00	0.
O2+HCO=CO+HO2	3.E+12	0.00	0.
HCO+M=CO+H+M	1.6E+14	0.00	14700.
CH3+O2=CH3O+O	7.E+12	0.00	25652.
CH3+OH=CH2O+H2	7.5E+12	0.00	0.
CH3O+M=CH2O+H+M	2.4E+13	0.00	28812.
CH3O+H=CH2O+H2	2.E+13	0.00	0.
CH3O+OH=CH2O+H2O	1.E+13	0.00	0.
CH3O+O=CH2O+OH	1.E+13	0.00	0.
CH3O+O2=CH2O+HO2	6.3E+10	0.00	2600.
CH3+O2=CH2O+OH	5.2E+13	0.00	34574.
CH3HCO+O=CH3+CO+OH	5.E+12	0.00	1900.
CH3HCO+OH=CH3+CO+H2O	1.E+13	0.00	0.
C3H6+O=CH3+CH3+CO	5.E+12	0.00	454.
C3H6+OH=CH3HCO+CH3	1.E+13	0.00	0.
C7H16+H=C7H15+H2	6.1E+14	0.00	8469.
C7H16+O=C7H15+OH	1.6E+14	0.00	4569.
C7H16+OH=C7H15+H2O	1.7E+13	0.00	957.
C7H15=CH3+C3H6+C3H6	3.7E+13	0.00	28708.

Table 1. Heptane kinetic scheme in CHEMKIN format.

For what concern inert heating and water vaporization refers to the fourth paragraph.
The volatiles release starts when the temperature of the particle reaches the devolatilization temperature and the water content is completely evaporated, and continues until the volatile fraction in consumed. The model used to calculate the rate of devolatilization is the single kinetic rate [14]. It assumes that the rate of devolatilization is first-order dependent on the amount of volatiles remaining in the particle.
After the volatile component is completely released, a surface reaction starts, following the stoichiometric requirement.
The kinetic/diffusion-limited rate model assumes that the surface reaction rate is determined either by kinetics or by diffusion rate. Here, the model of Baum and Street [15] and Field [16], is applied: a diffusion rate coefficient and a kinetic rate are weighted to determine char combustion rate. Chemical reaction on the internal surface and pore diffusion are taken into account in the kinetic rate. When the combustible fraction is totally burned, the residual continue the heating or cooling process.

5.1 Results

We have not simulated slurry particle break-up, but we have imagined introducing them already atomised, with a Rosin-Rammler diameter distribution (min $d=1*10^{-6}$ m, mean

d=4.5*10^{-5} m, max d=3*10^{-4} m, spread parameter=1.36). Recirculated gasses mass flow rate is 2480 kg/h, at 511 K, with the following mass composition:

CO_2 61.74%-- H_2O 30.83%-- O_2 3.17%-- N_2 4.26%

The mass flow rate of oxygen added is 1100kg/h. Coal water slurry flow rate is 509.01 kg/h with 28% by volume of water. Water vapour mass flow rate is 180 kg/h. Coal type used in the simulations has 25.04% of volatiles, 54% of char and 15.7% of ash (dry) with a low calorific value of 23.76 MJ/kg, while the ultimate analysis is: 66.10% C, 4.80% H, 6% O, 1% N and 1% S. The devolatilization temperature is 773 K, while in the devolatilization model the pre-exponential factor and activation energy are 2*10^5 and 7.4*10^7 J/kgmol. In the kinetic/diffusion surface combustion model the mass diffusion limited rate constant is 5*10^{-12}, the kinetic limited rate pre-exponential factor is 6.7 and kinetics limited rate activation energy is 1.138*10^8 J/kgmol. The stoichiometric ratio for char combustion is 2.67 (mass of oxygen/mass of carbon). The supposed reactions in gas phase are:

$$Volatiles + 2.46O_2 \rightarrow 0.633\ CO_2 + 2.118\ H_2O + 2.17\ CO + 0.071\ N_2$$

$$CO + 0.5\ O_2 \rightarrow CO_2$$

Char combustion reaction is:

$$C + O_2 \rightarrow CO_2$$

Combustion chamber has been considered non-adiabatic, with a heat transfer coefficient of 9 W/m^2K and a refrigerant temperature of 343 K. The operating pressure is 4 bar.
Four CFD simulations have been executed:

1. Standard operation (boundary conditions above)
2. Bigger granulometry (mean d=1*10^{-4} m)
3. Higher recirculated gasses temperature (773 K)
4. Higher recirculated gasses mass flow rate and temperature (5083 kg/h and 773 K)

The first three cases examined are fairly similar regarding the flow pattern: we can see the formation of two vortices externally respect furnace axis. Because of fuel energetic mass flow, introduced at high velocity, it cannot be slowed down adequately by recirculation vortices formed by swirled oxidant (fig. 5a). Also maximum temperatures reached are the same, about 1800 K (fig. 6 a,b,c, 7).

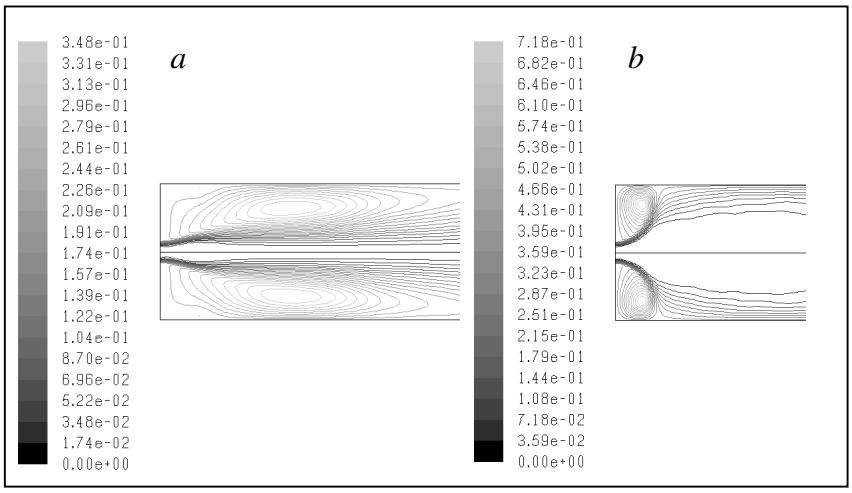

Figure 5. Stream function (kg/s). a) Case 1, Case 2, Case 3, b) Case 4.

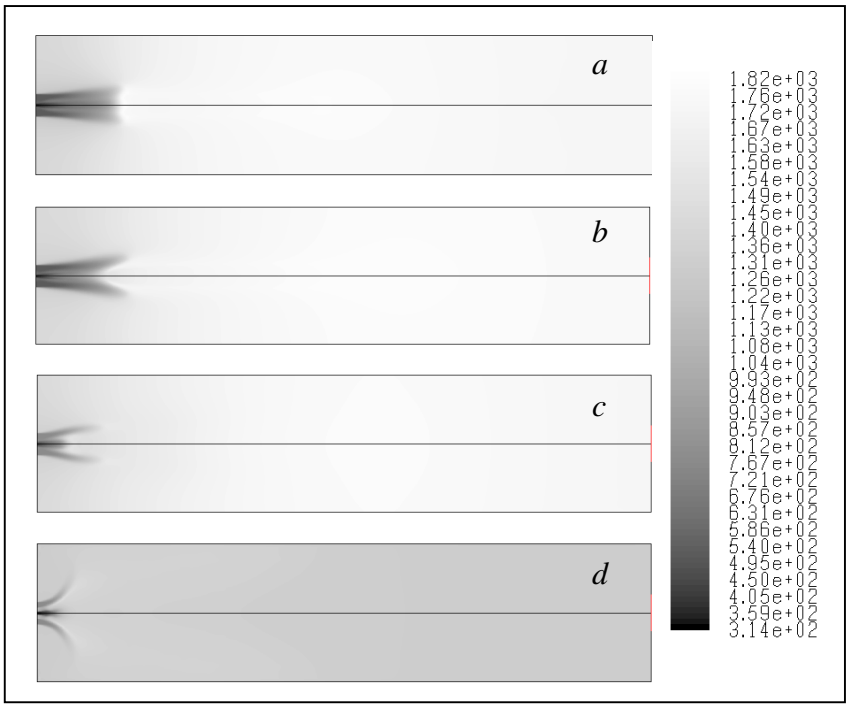

Figure 6. Temperature (K). a) Case 1, b) Case 2, c) Case 3, d) Case 4.

It is useful to remember that before volatiles release begin and, successively, char burns, particles water content must be evaporated. For case one, devolatilization happens between 0.6-0.7 m (fig. 8a) from inlet and successively burnout begins (fig. 9a), finishing at over one half of furnace. In the second case, the bigger particles size causes a wider devolatilization (fig. 8b) and a longer burnout (fig. 9b). For the third case, the higher inlet temperature determines a more rapid devolatilization and burnout, located between 0.25 and 0.65 m from inlet (fig. 8c, 9c).

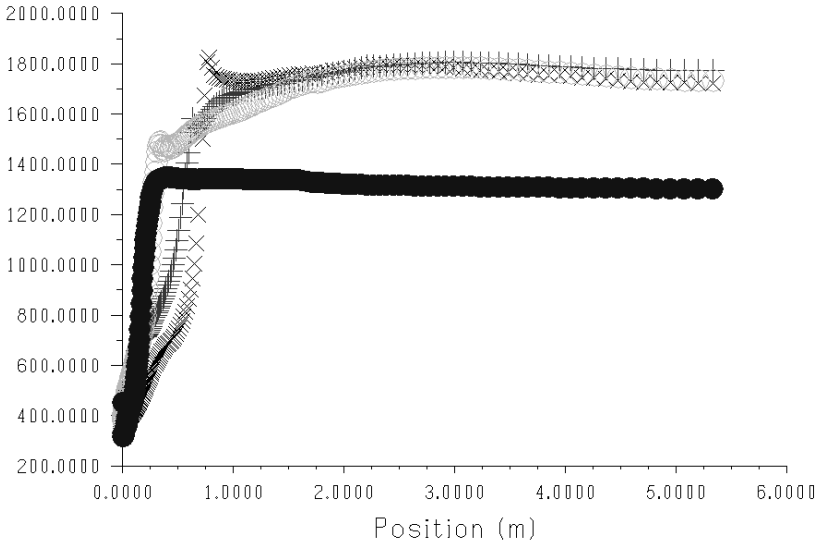

Figure 7. Axial temperature (K). + Case 1, x Case 2, o Case 3, • Case 4.

In the last case the flow pattern is completely different (fig. 5d). The two vortices are located in the left corner of the furnace. The augmented swirled oxidant flow rate introduced has sufficient energy to slow down fuel flow. In this working conditions, oxygen concentration in the oxidant is not larger than 18% in mass, while in the previous tests it reaches 32%. For this

reason, although sudden water evaporation and volatiles release (fig 8d), combustion is delayed and distributed in a wider zone, temperatures level are much lower (1500 K, fig. 6d) and temperature field is very uniform (fig. 7), looking like a mild combustion. In general, case 4 boundary conditions seam to guarantee the best performance in terms of flow field and therefore flame stability. Moreover, realize high temperatures in order to destruct possible pollutants, is not necessary in the case of coal water slurry as for generically waste fuel. In the other three cases, in particular velocity field plays an unfavourable role.

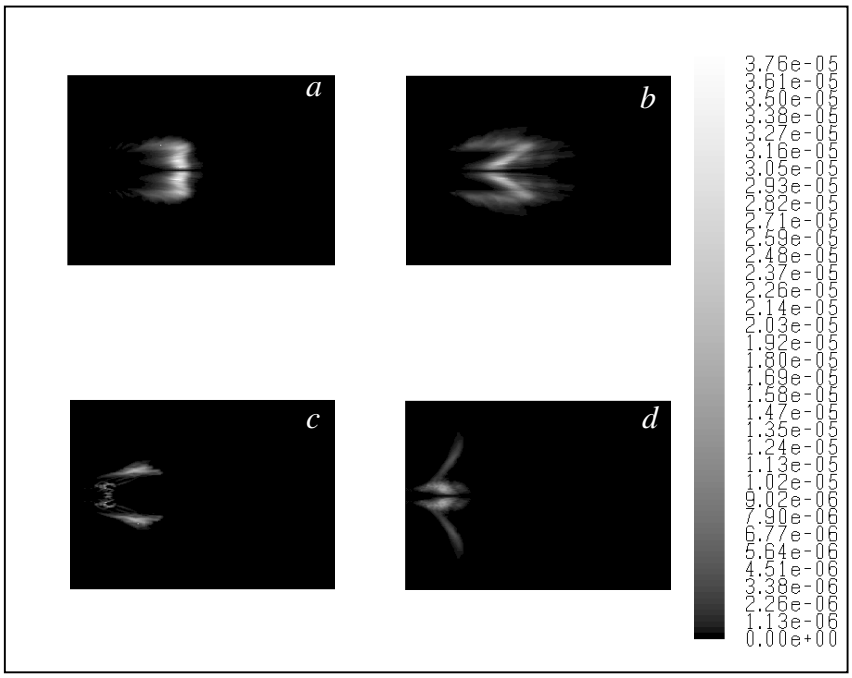

Figure 8. Volatiles emission rate (kg/s). a) Case 1, b) Case 2, c) Case 3, d) Case 4.

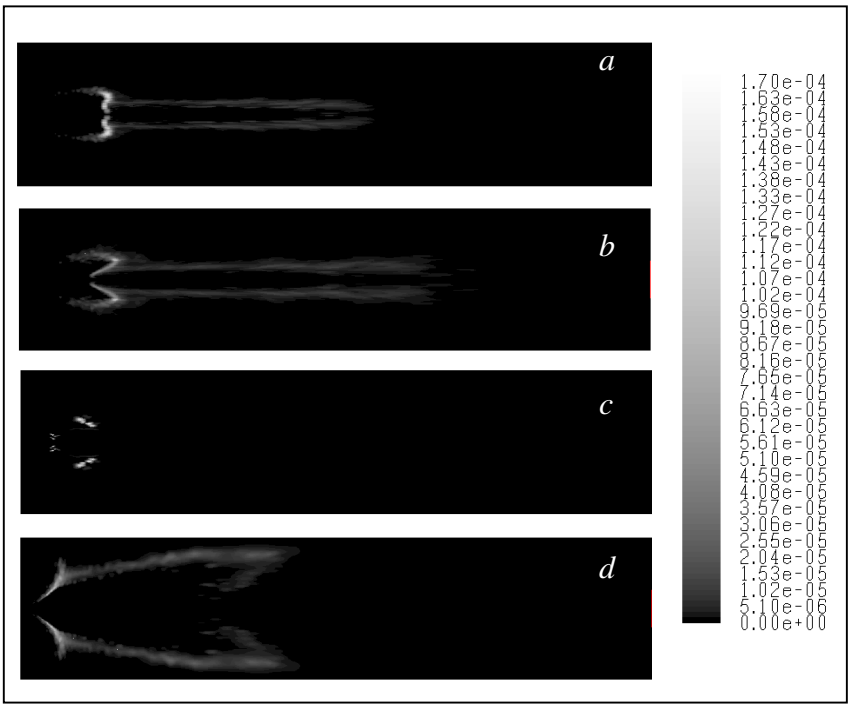

Figure 9. Char combustion rate (kg/s). a) Case 1, b) Case 2, c) Case 3, d) Case 4.

6 CONCLUSIONS

We have shown some simulations on an industrial reactor for disposal of industrial and hazardous waste fed with liquid fuel and slurry of pulverized coal. In the first case accurate simulations have been executed, using a detailed kinetic mechanism, in order to capture all the physical aspects involved and obtain reliable results. In the second case we have used a simple chemical model but, despite this, the results of the simulations give us some important indications as, for instance, the fact that the presence of water influences in decisive way the combustion process and the thermal exchange. The final goal will be the introduction of more detailed chemical models and the prediction of pollutants formation as, for example, nitrogen and sulphur oxides in both cases.

7 REFERENCES

[1] Launder B. E. and Spalding D. B., Lectures in Mathematical Models of Turbulence, Academic Press, London, England, 1972.

[2] Shih T.-H., Liou W. W., Shabbir A., Yang Z. and Zhu J., A New k-ε Eddy-Viscosity Model for High Reynolds Number Turbulent Flows–Model Development and Validation, Computers Fluids, 24(3):227-238, 1995.

[3] Chui E. H. and G. D. Raithby, 1993, Computation of Radiant Heat Transfer on a Non-Orthogonal Mesh Using the Finite-Volume Method, Numerical Heat Transfer Part B, 23:269-288.

[4] Coppalle A. and Vervisch P., The Total Emissivities of High-Temperature Flames, Combust. Flame, 49:101-108, 1983.

[5] Smith T. F., Shen Z. F. and Friedman J. N., Evaluation of Coefficients for the Weighted Sum of Gray Gases Model, J. Heat Transfer, 104:602-608, 1982.

[6] Morsi, S. A. and A. J. Alexander, 1972, An Investigation of Particle Trajectories in Two-Phase Flow Systems, J. Fluid Mech., 55(2):193-208.

[7] Haider A. and O. Levenspiel, 1989, Drag Coefficient and Terminal Velocity of Sphericaland Nonspherical Particles, Powder Technology, 58:63-70.

[8] Ranz W. E. and Marshall W. R. Jr., Evaporation from Drops, Part I. Chem. Eng. Prog., 48(3):141-146, March 1952.

[9] Ranz W. E. and Marshall W. R. Jr., Evaporation from Drops, Part II. Chem. Eng. Prog., 48(4):173-180, April 1952.

[10] Kuo K. K. Y., Principles of Combustion, John Wiley and Sons, New York, 1986.

[11] Liu A. B., D. Mather and R. D. Reitz, 1993, Modelling the Effects of Drop Drag and Breakup on Fuel Sprays, SAE Technical Paper 930072, SAE.

[12] Reitz R. D., 1987, Mechanisms of Atomization Processes in High-Pressure Vaporizing Sprays, Atomization and Spray Technology, 3:309-337.

[13] O'Rourke P. J., 1981, Collective Drop Effects on Vaporizing Liquid Sprays, PhD thesis, Princeton University, Princeton, New Jersey.

[14] Badzioch S. and Hawksley P. G. W., Kinetics of Thermal Decomposition of Pulverized Coal Particles, Ind. Eng. Chem. Process Design and Development, 9:521-530, 1970.

[15] Baum M. M. and Street P. J., Predicting the Combustion Behavior of Coal Particles, Combust. Sci. Tech., 3(5):231-243, 1971.

[16] Field M. A., Rate of Combustion Of Size-Graded Fractions of Char from a Low Rank Coal between 1200 K-2000 K, Combustion and Flame, 13:237-252, 1969.